Shape, orientation, and crystalline composition of silver islands on Si(111)

D. Wall
S. Tikhonov
S. Sindermann
D. Spoddig
C. Hassel
M. Horn-von Hoegen
F.-J. Meyer zu Heringdorf

Photoemission electron microscopy and spot profile analyzing low-energy electron diffraction have been used to study the temperature-dependent growth of Ag islands on a Si(111) surface. Depending on growth temperature, various island shapes can be formed. At low temperatures, polygonic islands are formed, consisting of both Ag(001) and Ag(111) crystal orientations. At higher temperatures, islands consist mostly of Ag(111) orientation and are predominantly of triangular shape. As the islands grow, it is possible that the crystalline composition of an island changes. We observed that Ag(001)-oriented areas convert into areas of Ag(111) orientation. The rotational orientation of the Ag islands with respect to the substrate is explained by a modified coincidence-site lattice approach.

Introduction

Silver is one of the most widely used materials for the study of fundamental material properties. For instance, Ag has been popular for diffusion experiments [1–8] and for studying metal-induced faceting [9–11]. However, silver is also important because of its dielectric properties. Stained-glass windows rely on the specific size-dependent plasmonic properties of Ag nanoparticles [12–14], and structured Ag films are commonly used to study light-metal interactions [15] in nonlinear photoemission and surface plasmon-enhanced photoemission [16–21].

Our interest in silver islands is based on the self-assembly of Ag on Si surfaces. If Ag is, for instance, deposited on 4° miscut Si(001) surfaces, thin (~100-nm) and long (>20-μm) nanowires form by self-assembly [8, 22]. These wires can then be contacted by electron beam (e-beam) lithography (EBL) and have been used for *in situ* electromigration experiments [23]. Surprisingly, the electromigration behavior of the self-assembled wires was qualitatively different from the known behavior of EBL-structured polycrystalline wires [24]. It was speculated that the grain boundaries in the polycrystalline wires are responsible for the changed behavior. It would thus be desirable to compare the electromigration of a single-crystalline wire to a wire containing a single grain boundary. Recently, Fujikawa et al. [25] have reported the self-assembly of Ag islands on Si(111) with both (001) and (111) crystalline areas and, naturally, a grain boundary between these areas. Such islands could be used as a starting material for the electromigration experiments. The self-assembly of Ag islands on Si(111), particularly the formation mechanism of bicrystalline islands, however, has to be understood in more detail. Here, we present a combined photoemission electron microscopy (PEEM) and spot profile analyzing low-energy electron diffraction (SPA-LEED) study to investigate the shape, the orientation relative to the substrate, and the crystallinity of self-assembled Ag islands on Si(111).

Experiments

The experiments were performed in an ultrahigh-vacuum (UHV) photoemission electron microscope (Elmitec PEEM III). PEEM was performed by illuminating the sample with ultraviolet light from a mercury discharge lamp. The samples were heated from the backside using electron bombardment. SPA-LEED measurements were performed in a separate UHV apparatus with resistive sample heating. Precision-oriented (better than 0.1°) Si(111) substrates were cleaned by standard flash annealing after degassing of the samples at 600°C in UHV for several hours. Ag was deposited from an e-beam-heated tantalum crucible in a homebuilt evaporation cell [26, 27]. Ag deposition occurred at elevated substrate temperatures (150°C–600°C) and

Digital Object Identifier: 10.1147/JRD.2011.2158761

©**Copyright** 2011 by International Business Machines Corporation. Copying in printed form for private use is permitted without payment of royalty provided that (1) each reproduction is done without alteration and (2) the Journal reference and IBM copyright notice are included on the first page. The title and abstract, but no other portions, of this paper may be copied by any means or distributed royalty free without further permission by computer-based and other information-service systems. Permission to republish any other portion of this paper must be obtained from the Editor.

0018-8646/11/$5.00 © 2011 IBM

was monitored either *in situ* with PEEM or after growth at an elevated temperature with SPA-LEED at room temperature. The sample temperature was measured with an infrared pyrometer (PEEM and SPA-LEED system) and a thermocouple (PEEM system). To analyze a larger number of islands, *ex situ* scanning electron microscopy (SEM) with a larger field of view was used. All electron backscatter diffraction (EBSD) measurements were carried out in a Leo 1530 Gemini scanning electron microscope equipped with an HKL Channel 5 EBSD system [28, 29]. The crystal structures of Si and Ag were taken from the HKL phase database [space group (SG) 225, lattice constant (LC)] and the Inorganic Crystal Structure Database (SG 227, LC), respectively. Our structures were suitable for automated EBSD analysis and were used here for indexing of the diffraction patterns (Kikuchi patterns) [29]. The indexing rate (i.e., the fraction of pixels in EBSD maps, of which the unit cell orientation could be successfully indexed) depends on the surface quality and can be close to 100%. Here, because of the Ag islands on the Si surface, the indexing rates of the raw EBSD maps are in the range of 95%.

As Ag is deposited onto a Si(111) surface, various reconstructions form, depending on the substrate temperature. At elevated temperatures, as the coverage exceeds one monolayer, Ag islands are formed in a Stranski-Krastanov type of growth on a $(\sqrt{3} \times \sqrt{3}) - R30^\circ$ [30, 31] reconstructed layer. After growth, several island shapes and islands of different crystallographic orientation have been observed. **Figure 1** shows some typical Ag island shapes on Si(111). At low temperatures [$T = 185^\circ$C in Figure 1(a) and $T = 240^\circ$C in Figure 1(b)], many islands consist of areas of both (001) and (111) orientations. The darker rectangular areas of the islands are of the (001) orientation, and the bright areas are of the (111) orientation, as was previously observed by Fujikawa et al. [25] and which was explained by a final-state effect [25, 32]. We confirmed the crystallographic orientation independently by EBSD. At higher growth temperatures, the (001) orientation becomes increasingly rare; instead, mostly polygonic islands with (111) composition form. The crystallographic composition is reflected in shapes with multiples of 60° angles at the perimeter of the islands. However, during growth at even higher temperatures, predominantly triangular islands, such as those in Figure 1(d), are observed.

The bottom panel in Figure 1 shows a SEM analysis of the gradual transition from polygonic and hexagonally shaped islands to triangular islands as a function of growth temperature. At growth temperatures above 500°C, the transition from polygonic to triangular islands starts, with more than 50% of the islands exhibiting a triangular shape at temperatures above 620°C. We therefore conclude that Ag(111) islands on Si(111) prefer a triangular shape but that their formation is kinetically limited at lower temperatures.

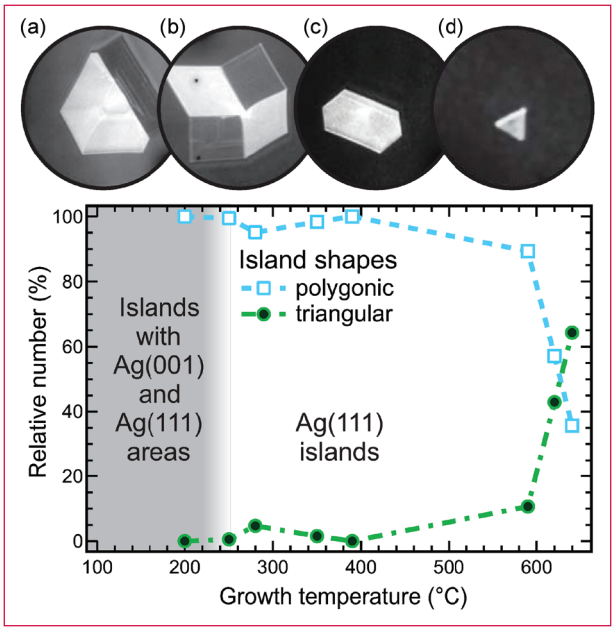

Figure 1

Ag islands. (a)–(d) Typical shapes of Ag islands grown on Si(111), each recorded using PEEM with a field of view of 50 μm. Growth was performed at different temperatures. (a) $T = 185^\circ$C. (b) $T = 240^\circ$C. (c) $T = 220^\circ$C. (d) $T = 530^\circ$C. The darker areas in (a) and (b) resemble the Ag(001) areas. (Bottom panel) Distribution of island shapes as a function of temperature. Polygonic and mostly hexagonal island shapes have been observed up to $T = 620^\circ$C. At higher temperatures, triangular shapes dominate. Ag(001) areas are not included in the bottom panel, as they are predominantly formed at lower temperatures.

Even at higher growth temperatures, when the islands are of the (111) type and predominantly have triangular shapes, they exhibit different orientations with respect to the substrate lattice. Multiples of 60° are certainly possible, but also rotation angles of around 19° and smaller rotation angles are present in significant numbers. To retrieve the orientation of a large number of islands relative to the substrate, SPA-LEED measurements were performed. With an e-beam size of approximately 1 mm, the diffraction pattern represents an average of a sufficiently large area on the sample. **Figure 2(a)** shows a typical SPA-LEED pattern at an electron energy of 109.5 eV of a Si(111) surface with Ag islands grown in a temperature regime of $T = 150^\circ$C to $T = 200^\circ$C. The unit cell of the $(\sqrt{3} \times \sqrt{3})$ reconstructed wetting layer and the integer-order spots of the Si substrate are indicated. The dominant feature of the SPA-LEED pattern is a ring around the (00) spot. The radius of the ring corresponds to the Ag(111) LC, i.e., the intensity modulation on the ring reflects the distribution of the crystalline orientation of the Ag islands with respect to the substrate. At 150°C–200°C, the rotational ordering of the islands shows a broad distribution of orientations. Nevertheless,

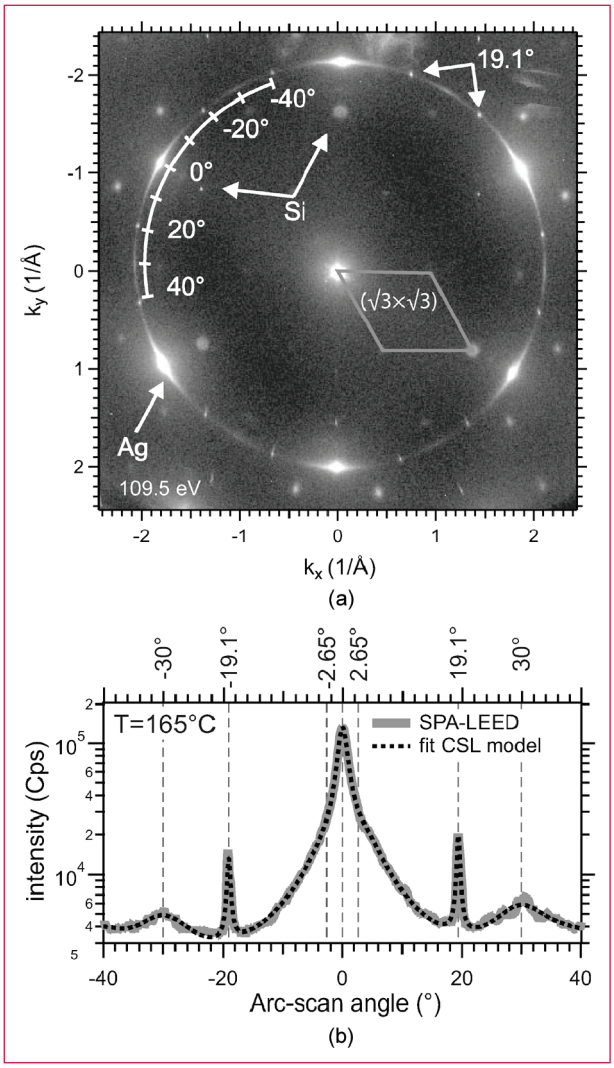

Figure 2

SPA-LEED pattern and arc scan. (a) Typical SPA-LEED pattern for Ag islands grown at $T = 150°C$ to $T = 200°C$ on Si(111). The intensity is logarithmically scaled. Some of the Si first-order diffraction spots are labeled for reference. In between the islands, a $(\sqrt{3} \times \sqrt{3})$ reconstruction is present. The ring has a diameter corresponding to the size of the reciprocal Ag(111) LC, and the intensity modulation on the ring reflects the rotational distribution of the crystals with respect to the substrate. (b) Arc scan along the indicated part of the ring. The multipeak Lorentzian fit included in (b) is fixed to the angles from a CSL model. (Dashed lines) Position of the fitted peaks.

the Ag crystal lattice locks in at certain rotation angles with respect to the substrate orientation. In SPA-LEED, this is reflected in the small bright spots at a rotation angle of around $\pm 19°$ relative to the Si integer-order spots and the main Ag crystal orientation.

We explain the specific rotation angles of the Ag crystal lattice in a coincidence-site lattice (CSL) model [33–35]. In the CSL model, two lattices are rotated with respect to each other, and the overlap in terms of the number of coincidence sites of the two lattices is calculated. Although such a model has analytical solutions for homoepitaxial systems [36, 37], for heteroepitaxy, the lattice sites usually do not reach perfect coincidence because of the different LCs. As such, a measure for the coincidence is needed. We calculated the distance between each lattice site $\vec{r}_i$ of a (rotated) Ag lattice site with respect to lattice sites $\vec{r}_j$ of a Si lattice. For both lattices, the simplest case of bulk-terminated structures is assumed, as little is known about the exact geometry at the interface. For the classical CSL, $\Sigma =$ size of the CSL unit cell/size of the crystal unit cell is a parameter that is inversely proportional to how many binding sites per area are possible, and this quantity is a direct measure of how strong the binding of a certain rotation is. The strength of crystal binding, however, does depend not only on the number of bonds per area, as in the classical CSL theory, but also on the bond distance. As the binding is of covalent nature, we added a simple electrostatic approximation and quality factor $Q = \sum_{i=0,j=0}^{N,M}(1/(\vec{r}_i - \vec{r}_j)^2)$ with an inversely quadratic dependence of the lattice site distance as a measure of how well the lattices coincide. N and M are the numbers of lattice sites of the substrate and the island, respectively. It is important to note that the resulting angles for rotational domains with high Q do not critically depend on the assumed quadratic dependence of the electrostatic potential, and other powers yield similar results. We calculated both quality factor Q and classic CSL parameter Σ for each rotation angle. To determine the size of the CSL unit cell for the calculation of Σ, we assumed that the two lattice sites coincide if their distance is ≤ 20 pm, and we calculated Σ with respect to the adsorbate lattice unit cell.

A combination of both parameters, i.e., high Q and low Σ, leads to a theoretical prediction of the preferred rotation angles. **Figure 2(b)** shows an arc scan along the line indicated in Figure 2(a). The dotted line in Figure 2(b) is a multi-Lorentzian peak fit in which the peak positions were taken from our CSL model. We observe rotation angles of $\pm 19.1°$ and $\pm 30°$. The broad appearance of the peak at 0° can be explained by the superposition of three possible rotation angles 0° and $\pm 2.65°$. The observed SPA-LEED spots at a rotation angle of $\pm 30°$ are not dominant but can be explained in the CSL model as well. The 30° spot positions also correspond to Ag islands with (001) orientation since Ag(001) islands with fourfold symmetry have the same atomic row distance of approximately 2.5 Å as the Ag(111) islands. The Ag(001) areas can therefore easily align with each of the six possible orientations on the substrate and give rise to intensities at the rotation angles of $n \cdot 30°$, with $n \in \mathbb{N}$. The weak intensity of the spots at $\pm 30°$ allows us to conclude that only a small fraction of the surface is covered by Ag(001).

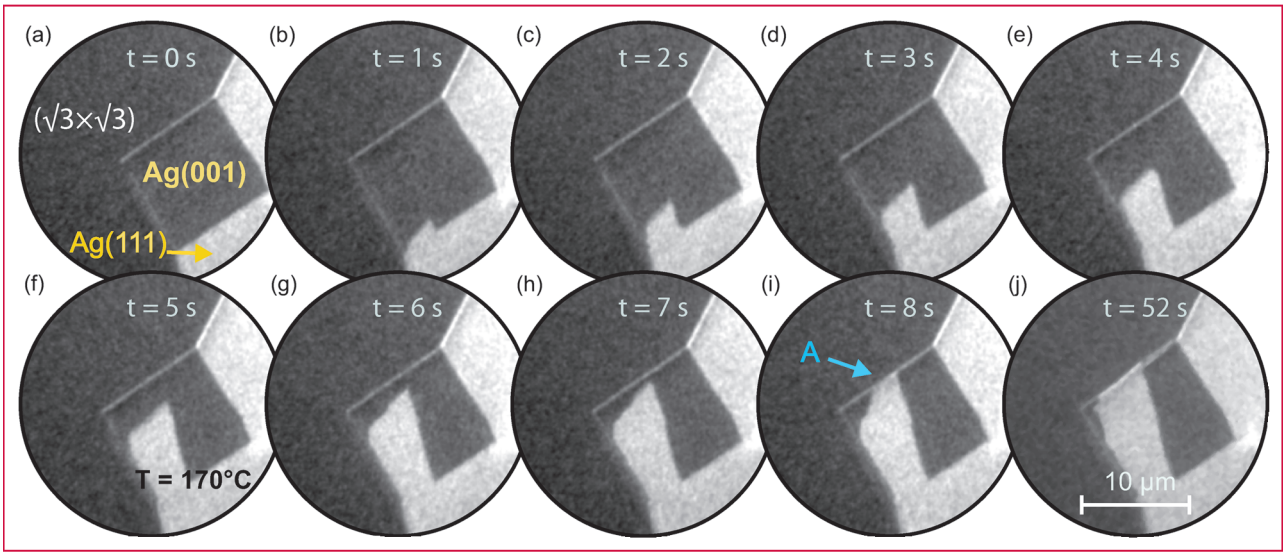

Figure 3

PEEM image sequence recorded at a rate of one image per second during the growth of a large Ag island with both (dark) (001) and (bright) (111) composition. (a) Typical rectangular shape of the (001)-oriented areas after growth for several minutes. (b)–(i) Quick brightness change of a large part of the (001)-oriented region. The converted area can no longer be distinguished from the (111)-oriented region. (j) After the contrast change has reached the opposite edge of the Ag(001) area, the change dramatically slows down, as only little change can be observed until $t = 52$ seconds. The deposition started at $t = -205$ seconds.

Two of the dominant rotation angles from the CSL model ($\pm 10.85°$ and $\pm 14.4°$) were not necessary to explain the arc scan and were therefore removed from the fit. Apparently, the fraction of the $\pm 10.85°$ and $\pm 14.4°$ rotated islands on the surface is negligibly small.

One would naturally assume that the crystallographic composition, i.e., (001) or (111), of a single island is determined by the orientation that the island nucleates in. However, we never observed pure (001) islands in PEEM; instead, (001) areas were always in contact with (111) areas. Furthermore, when Ag islands with (001) and (111) composition grow, the crystallographic composition can change to yield a pure (111) island. **Figure 3(a)** shows a typical island with Ag(001) and Ag(111) composition that we observe when Ag is deposited between $T = 150°C$ and $T = 200°C$ sample temperatures. The Ag(001) region is dark and rectangular, and the angles between the (001)- and (111)-oriented regions are typical for a combination of fourfold and sixfold symmetry. At $t = 0$ seconds, the island has already grown for several minutes to reach the shown size. Then, within seconds [see **Figure 3(b)–3(i)**], a contrast change of an area of several 10 μm^2 occurs and decreases the size of the typical (001) region. **Figure 3(j)** shows the situation at $t = 52$ seconds. After the front of the contrast change has reached the opposing end of the Ag(001) area ["A" in Figure 3(i)], the rate of change slows down dramatically. Still, it is usually possible to convert the entire dark area. We also observed the occurrence of such a transformation as a result of a temperature increase.

As several islands on several samples exhibited the same behavior, further *ex situ* analysis of the converted regions was performed. In particular, some of the converted islands were analyzed by EBSD, which confirmed that the originally (001)-oriented areas are of (111) orientation after the conversion. However, grain boundaries within the islands and small-angle grain boundaries are possible and were also observed with EBSD.

Conclusion

In conclusion, Ag islands on Si(111) have a complex composition, and the islands exhibit various shapes, crystallographic orientations, and grain boundaries. The orientation and shape are predominantly influenced by growth temperature. At slightly elevated temperatures, bicrystalline islands form with (often) irregular shapes and both (001)- and (111)-oriented areas. An increase in growth temperature results in pure (111) islands, the shape of which becomes increasingly triangular with growth temperature. Interestingly, in the bicrystalline islands, a conversion of (001) areas into areas of (111) composition can be triggered by temperature or randomly occurs during deposition. So far, we can only speculate about the origin of the conversion, but as the conversion can be triggered by thermal expansion and seems to be linked to the overall (001) area

of the island, stress effects are likely. After the conversion, a (111)-oriented island is observed, exhibiting 90° angles at the edges.

With regard to the orientation of the islands with respect to the substrate, we have found that the islands are often rotated by ±2.65° and that even islands exist with a rotation angle of ±19.1° with respect to the substrate lattice. The specific values of the observed angles can be understood in terms of a simple CSL model.

In many cases, however, we have not only observed the rotation of entire islands but also found Ag(111) islands that are composed of differently rotated areas. The different areas are separated by grain boundaries. The shape of such islands appears to have "crooked" edges, and the different areas cannot be easily distinguished by SEM or PEEM but can be identified by EBSD and other microcrystallographic methods. As a nonscanning *in situ* method, LEEM could be the ideal tool to study the dynamics of the recrystallization of the Ag(001) areas in future studies.

Acknowledgments

The authors thank M. Farle for access to the EBSD system. This work was supported by the Deutsche Forschungsgemeinschaft through Grant SFB 616 "Energy Dissipation at Surfaces."

References

1. K. Morgenstern, G. Rosenfeld, and G. Comsa, "Local correlation during Ostwald ripening of two-dimensional islands on Ag(111)," *Surf. Sci.*, vol. 441, no. 2/3, pp. 289–300, Nov. 1999.
2. L. Pedemonte, R. Tatarek, M. Vladiskovic, and G. Bracco, "Anisotropic self-diffusion on Ag(110)," *Surf. Sci.*, vol. 507-510, pp. 129–134, Jun. 2002.
3. F. Hontinfinde, R. Ferrando, and A. C. Levi, "A numerical study of the epitaxial growth of silver on silver (110)," *Phys. A: Stat. Theor. Phys.*, vol. 248, no. 3/4, pp. 288–304, Jan. 1998.
4. D. Wall, I. Lohmar, K. R. Roos, J. Krug, M. Horn-von Hoegen, and F.-J. Meyer zu Heringdorf, "Imaging diffusion fields on a surface with multiple reconstructions: Ag/Si(111)," *New J. Phys.*, vol. 12, no. 10, article no. 103019, 2010.
5. K. R. Roos, K. L. Roos, I. Lohmar, D. Wall, J. Krug, M. Horn-von Hoegen, and F.-J. Meyer zu Heringdorf, "A real-time view of mesoscopic surface diffusion," *Phys. Rev. Lett.*, vol. 100, no. 1, article no. 016103, Jan. 2008.
6. K. R. Roos and U. C. Tringides, "Low-temperature, flux-independent epitaxy in Ag/Si(111)," *Surf. Sci.*, vol. 302, no. 1/2, pp. 37–48, Jan. 1994.
7. M. Stanley, C. Papageorgopoulos, K. R. Roos, and M. C. Tringides, "RHEED studies of interlayer diffusion in the submonolayer growth regime on Ag/Ag(111)," *Surf. Sci.*, vol. 355, no. 1–3, pp. L264–L270, Jun. 1996.
8. D. Wall, S. Sindermann, K. R. Roos, M. Horn-von Hoegen, and F.-J. Meyer zu Heringdorf, "The influence of anisotropic diffusion on Ag nanowire formation," *J. Phys.: Condens. Matter*, vol. 21, no. 31, article no. 314023, Aug. 2009.
9. S. Fölsch, D. Winau, G. Meyer, K. Rieder, M. Horn-von Hoegen, T. Schmidt, and M. Henzler, "Ag-induced multistep formation on Si(001)," *Appl. Phys. Lett.*, vol. 67, no. 15, pp. 2185–2187, Oct. 1995.
10. T. Nabbefeld, C. Wiethoff, F.-J. Meyer zu Heringdorf, and M. Horn-von Hoegen, "Silver induced faceting of Si(112)," *Appl. Phys. Lett.*, vol. 97, no. 4, article no. 041905, Jul. 2010.
11. A. Meier, P. Zahl, R. Vockenroth, and M. Horn-von Hoegen, "Step arrangement control of vicinal Si(001) by Ag adsorption," *Appl. Surf. Sci.*, vol. 123/124, pp. 694–698, Jan. 1998.
12. H. A. Atwater and A. Polman, "Plasmonics for improved photovoltaic devices," *Nat. Mater.*, vol. 9, no. 3, pp. 205–213, Mar. 2010.
13. J. P. Kottmann, O. J. F. Martin, D. R. Smith, and S. Schultz, "Plasmon resonances of silver nanowires with a nonregular cross section," *Phys. Rev. B, Condens. Matter*, vol. 64, no. 23, article no. 235402, Dec. 2001.
14. S. Lal, S. Link, and N. J. Halas, "Nano-optics from sensing to waveguiding," *Nat. Photon.*, vol. 1, no. 11, pp. 641–648, Nov. 2007.
15. M. Cinchetti, A. Gloskovskii, S. A. Nepjiko, G. Schönhense, H. Rochholz, and M. Kreiter, "Photoemission electron microscopy as a tool for the investigation of optical near fields," *Phys. Rev. Lett.*, vol. 95, no. 4, article no. 047601, Jul. 2005.
16. M. Aeschlimann, C. A. Schmuttenmaer, H. E. Elsayed-Ali, R. J. D. Miller, J. Cao, Y. Gao, and D. A. Mantell, "Observation of surface enhanced multiphoton photoemission from metal surfaces in the short pulse limit," *J. Chem. Phys.*, vol. 102, no. 21, pp. 8606–8613, Jun. 1995.
17. M. Bauer and M. Aeschlimann, "Dynamics of excited electrons in metals, thin films and nanostructures," *J. Electron Spectrosc. Relat. Phenom.*, vol. 124, no. 2/3, pp. 225–243, Jul. 2002.
18. A. Kubo, K. Onda, H. Petek, Z. Sun, Y. S. Jung, and H. K. Kim, "Femtosecond imaging of surface plasmon dynamics in a nanostructured silver film," *Nano Lett.*, vol. 5, no. 6, pp. 1123–1127, Jun. 2005.
19. A. Kubo, N. Pontius, and H. Petek, "Femtosecond microscopy of surface plasmon polariton wave packet evolution at the silver/vacuum interface," *Nano Lett.*, vol. 7, no. 2, pp. 470–475, Feb. 2007.
20. L. I. Chelaru and F.-J. Meyer zu Heringdorf, "In situ monitoring of surface plasmons in single-crystalline Ag-nanowires," *Surf. Sci.*, vol. 601, no. 18, pp. 4541–4545, Sep. 2007.
21. F.-J. Meyer zu Heringdorf, L. I. Chelaru, S. Möllenbeck, D. Thien, and M. Horn-von Hoegen, "Femtosecond photoemission microscopy," *Surf. Sci.*, vol. 601, no. 20, pp. 4700–4705, Oct. 2007.
22. K. R. Roos, K. L. Roos, M. Horn-von Hoegen, and F.-J. Meyer zu Heringdorf, "High temperature self-assembly of Ag wires on vicinal Si(001)," *J. Phys.: Condens. Matter*, vol. 17, pp. S1407–S1447, 2005.
23. M. R. Kaspers, A. M. Bernhart, F.-J. Meyer zu Heringdorf, G. Dumpich, and R. Möller, "Electromigration and potentiometry measurements of single-crystalline Ag nanowires under UHV conditions," *J. Phys.: Condens. Matter*, vol. 21, no. 26, article no. 265601, Jul. 2009.
24. B. Stahlmecke, F.-J. Meyer zu Heringdorf, L. Chelaru, M. Horn-von Hoegen, G. Dumpich, and K. R. Roos, "Electromigration in self-organized single-crystalline silver nanowires," *Appl. Phys. Lett.*, vol. 88, no. 5, article no. 053122, Jan. 2006.
25. Y. Fujikawa, T. Sakurai, and R. M. Tromp, "Micrometer-scale band mapping of single silver islands in real and reciprocal space," *Phys. Rev. B, Condens. Matter*, vol. 79, no. 12, article no. 121401, Mar. 2009.
26. P. Kury, R. Hild, D. Thien, H.-L. Günter, F.-J. Meyer zu Heringdorf, and M. Horn-von Hoegen, "Compact and transferable threefold evaporator for molecular beam epitaxy in ultrahigh vacuum," *Rev. Sci. Instrum.*, vol. 76, no. 8, article no. 083906, Aug. 2005.
27. F.-J. Meyer zu Heringdorf and A. C. Belton, "Flexible microprocessor-based evaporation controller," *Rev. Sci. Instrum.*, vol. 75, no. 12, pp. 5288–5292, Dec. 2004.
28. D. J. Dingley and V. Randle, "Microtexture determination by electron back-scatter diffraction," *J. Mater. Sci.*, vol. 27, no. 17, pp. 4545–4566, Sep. 1992.
29. R. A. Schwarzer, "Automated crystal lattice orientation mapping using a computer-controlled SEM," *Micron*, vol. 28, no. 3, pp. 249–265, Jun. 1997.

30. Y. Ding, C. Chan, and K. Ho, "Structure of the $(\sqrt{3} \times \sqrt{3}) - R30^\circ$ Ag/Si(111) surface from first-principles calculations," *Phys. Rev. Lett.*, vol. 67, no. 11, pp. 1454–1457, Sep. 1991.
31. K. Wan, X. Lin, and J. Nogami, "Surface reconstructions in the Ag/Si(111) system," *Phys. Rev. B, Condens. Matter*, vol. 47, no. 20, pp. 13 700–13 712, May 1993.
32. A. Otto and B. Reihl, "Band-structure effects in secondary-electron-emission and absorbed-current spectra of (111), (100), and (110) surfaces of silver," *Phys. Rev. B, Condens. Matter*, vol. 41, no. 14, pp. 9752–9755, May 1990.
33. S. Ranganathan, "On the geometry of coincidence-site lattices," *Acta Crystallogr.*, vol. 21, pp. 197–199, Aug. 1966.
34. M. Baake, *Solution of the Coincidence Problem in Dimensions $d \leq 4$*, arxiv:math.MG/0605222 v1
35. D. H. Warrington, "The coincidence site lattice (CSL) and grain boundary (DSC) dislocations for the hexagonal lattice," *J. Phys. Colloques*, vol. 36, pp. C4-87–C4-95, 1975.
36. H. Grimmer, W. Bollmann, and D. H. Warrington, "Coincidence-site lattices and complete pattern-shift in cubic crystals," *Acta Crystallogr. Sect. A*, vol. 30, no. 2, pp. 197–207, Mar. 1974.
37. P. A. B. Pleasants, M. Baake, and J. Roth, "Planar coincidences for N-fold symmetry," *J. Math. Phys.*, vol. 37, no. 2, pp. 1029–1058, Feb. 1996.

Received October 28, 2010; accepted for publication February 22, 2011

Dirk Wall *Department of Physics and Center for Nanointegration Duisburg-Essen (CeNIDE), Universität Duisburg-Essen, 47057 Duisburg, Germany (dirk.wall@uni-due.de).*

Sergey Tikhonov *Department of Physics and Center for Nanointegration Duisburg-Essen (CeNIDE), Universität Duisburg-Essen, 47057 Duisburg, Germany (tikhonov@gmx.net).*

Simon Sindermann *Department of Physics and Center for Nanointegration Duisburg-Essen (CeNIDE), Universität Duisburg-Essen, 47057 Duisburg, Germany (simon.sindermann@uni-due.de).*

Detlef Spoddig *Department of Physics and Center for Nanointegration Duisburg-Essen (CeNIDE), Universität Duisburg-Essen, 47057 Duisburg, Germany (detlef.spoddig@uni-due.de).*

Christoph Hassel *Department of Physics and Center for Nanointegration Duisburg-Essen (CeNIDE), Universität Duisburg-Essen, 47057 Duisburg, Germany (christoph.hassel@uni-due.de).*

Michael Horn-von Hoegen *Department of Physics and Center for Nanointegration Duisburg-Essen (CeNIDE), Universität Duisburg-Essen, 47057 Duisburg, Germany (horn-von-hoegen@uni-due.de).*

F.-J. Meyer zu Heringdorf *Department of Physics and Center for Nanointegration Duisburg-Essen (CeNIDE), Universität Duisburg-Essen, 47057 Duisburg, Germany (meyerzh@uni-due.de).*